PHYSICAL REVIEW A **83**, 031401(R) (2011)

Angle-resolved photoelectron spectroscopy of sequential three-photon triple ionization of neon at 90.5 eV photon energy

A. Rouzée,[1] P. Johnsson,[2] E. V. Gryzlova,[3,4] H. Fukuzawa,[3] A. Yamada,[3] W. Siu,[1] Y. Huismans,[1] E. Louis,[5] F. Bijkerk,[5,6] D. M. P. Holland,[7] A. N. Grum-Grzhimailo,[4] N. M. Kabachnik,[4] M. J. J. Vrakking,[1,8] and K. Ueda[3]

[1]*FOM Institute, Amolf, Science Park 113, NL-1098 XG Amsterdam, The Netherlands*

[2]*Lund University, Department of Physics, P.O. Box 118, SE-221 00 Lund, Sweden*

[3]*Institute of Multidisciplinary Research for Advanced Materials, Tohoku University, Sendai 980-8577, Japan*

[4]*Institute of Nuclear Physics, Moscow State University, Moscow 119991, Russia*

[5]*FOM Institute for Plasma Physics Rijnhuizen, Edisonbaan 14, NL-3439 MN Nieuwegein, The Netherlands*

[6]*MESA+ Institute for Nanotechnology, University of Twente, P.O. Box 217, NL-7500 AE, Enschede, The Netherlands*

[7]*STFC, Daresbury Laboratory, Warrington, Cheshire WA4 4AD, UK*

[8]*Max Born Institute, Max-Born-Strasse 2a, D-12489 Berlin, Germany*

(Received 12 November 2010; published 18 March 2011)

Multiple photoionization of neon atoms by a strong 13.7 nm (90.5 eV) laser pulse has been studied at the FLASH free electron laser in Hamburg. A velocity map imaging spectrometer was used to record angle-resolved photoelectron spectra on a single-shot basis. Analysis of the evolution of the spectra with the FEL pulse energy in combination with extensive theoretical calculations allows the ionization pathways that contribute to be assigned, revealing the occurrence of sequential three-photon triple ionization.

DOI: 10.1103/PhysRevA.83.031401 PACS number(s): 32.80.Fb, 32.80.Hd

The development of free electron lasers (FELs) emitting radiation in the extreme ultraviolet and the x-ray spectral range heralds a new era in the study of nonlinear processes at high photon frequency. Using these new sources (FLASH in Germany, SPring-8 in Japan, and LCLS in the USA), previously unexplored regimes of atomic and molecular strong field ionization become accessible. In the first experiments [1–3] strongly nonlinear multiple ionization of atoms has already been observed. Since mainly multiply charged ions were detected, it was impossible to unambiguously identify the ionization mechanisms. Accordingly, the interpretation of some of these experiments is still under debate [4,5], and the main question is whether the experimental results can be understood without introducing new concepts, e.g., collective effects, in the description of the multiphoton multiple ionization at high frequencies. In the simplest case of two-photon double ionization (2PDI) two basic mechanisms have been established: direct (nonsequential) ionization, where both photons are absorbed simultaneously, and sequential ionization, where, after absorption of a first photon and emission of the first electron, intermediate ionic states are formed that are further ionized by a second photon. In order to disentangle the ionization mechanisms, a number of experimental techniques have so far been used, which include measurements of ionic charge state distributions [6], energy- and angle-resolved electron spectroscopy [7,8], measurements of recoil-ion-momentum distributions [9–12], and kinematically complete experiments using a reaction microscope [8]. Together with extensive accompanying theoretical work (e.g., Ref. [13] and references therein) these experiments have significantly advanced our understanding of 2PDI. In particular it was established, as first predicted theoretically [14], that sequential ionization is dominant if the photon energy is larger than the binding energy of the singly charged ion.

As a logical next step in studies of multiphoton multiple ionization in the high-frequency regime, we report the first observation of sequential three-photon triple ionization (3PTI) of neon atoms, based on a measurement of angle-resolved photoelectron spectra using the velocity map imaging technique [15]. Strong field triple ionization is much more complicated than double ionization due to the larger number of processes that can contribute. Therefore, although triply charged ions have been reported [1,2,9], individual pathways have not previously been identified. To overcome difficulties associated with stochastic shot-to-shot fluctuations in the energy of the FEL pulses, the velocity map electron images were recorded on a shot-to-shot basis together with the photon beam intensity measured using the in-house gas monitor detector and then accordingly sorted [16]. Together with the theoretical analysis this allowed us to identify the sequential 3PTI process. Both 3PTI and 2PDI were observed.

In the experiments, FLASH was operated in single-bunch mode at a repetition rate of 5 Hz, delivering linearly polarized laser pulses at 90.5 eV photon energy ($\lambda = 13.7$ nm), with a pulse duration estimated around 20 fs, and an average pulse energy of 40 μJ. The experiment was performed in a secondary focus of the BL2 beamline, where an in-line refocusing chamber composed of two multilayer mirrors [17] was used to focus the FEL beam to a spot size of less than 100 μm. The intensity of the FEL after reflection by the mirrors of the refocusing chamber was estimated to be 1.0×10^{13} W/cm^2. Before entering the interaction chamber, the FEL beam passed through a light baffle consisting of three skimmers with 4.4, 5, and 4 mm diameters, which were used to remove the majority of the scattered light specularly and nonspecularly reflected by the two mirrors. In the interaction region, the FEL beam crossed an atomic beam of neon at the center of a velocity map imaging spectrometer (VMIS). Electrons from ionization of the atoms by the FEL light were accelerated toward a position-sensitive detector consisting of a set of microchannel plates (MCPs) followed by a phosphor screen, and recorded using a gated CCD camera synchronized

to the arrival of the FEL pulse in the interaction chamber. A 200 ns electrical gate pulse was applied to the back of the MCPs. The measured two-dimensional (2D) projection allows the three-dimensional (3D) momentum distribution of the ejected electrons to be obtained using a mathematical inversion procedure. The retrieved 3D momentum distribution at each electron energy was described by the following expression:

$$W(E_e,\vartheta) = \frac{W_0(E_e)}{4\pi}\left[1+\sum_{k=2}^{k_{\max}}\beta_k(E_e)P_k(\cos\vartheta)\right], \qquad (1)$$

where $W_0(E_e)$ is the angle-integrated intensity, $\beta_k(E_e)$ (k = even) are anisotropy parameters at kinetic energy E_e, $P_k(x)$ is the Legendre polynomial of order k, and ϑ is the polar angle with respect to the laser polarization axis.

Figures 1(a) and 1(b) show the experimentally measured 2D electron image and a 2D slice through the retrieved 3D photoelectron momentum distribution (obtained after inversion). The momentum distribution contains a large number of contributions that are indicated in the angle-integrated photoelectron spectrum shown in Fig. 1(c). The strong line at 69.0 eV originating from single ionization of Ne to the ground ionic state, Ne $2p^6 \rightarrow \mathrm{Ne}^+$ $2p^5$, was used for calibration of the photoelectron energy axis. According to available spectroscopic data [18], the photoelectron spectrum in the regions of 40–52 and 13–32 eV should be dominated by the 2PDI and the 3PTI, respectively. However, more than one process may contribute to a certain line, since photoelectrons originating from different ion charge states and from ionization of $2s$ and $2p$ subshells can have very similar energies that cannot experimentally be resolved due to the finite energy resolution ($\Delta E_e/E_e \approx 2\%$) of the VMIS and the spectral fluctuations ($\Delta\lambda/\lambda \approx 1\%$–$3\%$) of the FEL.

In order to disentangle the ionization pathways, the FEL pulse energy dependence of each photoelectron peak was determined, exploiting the sorting procedure described above. The photoelectron spectra were sorted using a 2 μJ step in the FEL pulse energy. Figure 1(d) displays the evolution of the electron kinetic energy distribution, measured along the laser polarization, with the FEL pulse energy. The pulse energy dependence of individual peaks was fitted according to $S \sim E_{\mathrm{FEL}}^{\nu}$ [see Fig. 1(e) and the labels in Fig. 1(c)], where ν provides a lower limit on the number of FEL photons involved in a certain pathway. Thus the 69.0 eV line originates from single-photon absorption, whereas the 50.2 and 4.5 eV lines arise from the absorption of two and three photons, respectively. Deviations of ν from integer values are due to the fact that at high laser intensity saturation may be achieved.

In Figs. 2 and 3 a comparison of selected parts of the angle-resolved photoelectron spectrum with numerical simulations is presented. The theoretical description is based on a recently developed stepwise ionization model, where each subsequent photon interacts with an ionic intermediate state formed at a preceding step. This approach, in combination with the statistical tensor formalism [19], was previously successfully applied to sequential 2PDI from the outer p shells of noble gas atoms [8,20,21] and three-photon resonantly enhanced sequential double ionization of argon [22]. Within this model, anisotropy in the photoelectron emission and alignment of the intermediate states are fully taken into account. The photoionization amplitudes for each of the steps were calculated in the dipole approximation using the multiconfiguration Hartree-Fock method [23]. Further details of the calculations and the formalism will be given elsewhere. We note that in the particular case of p-shell photoionization in a nonrelativistic approximation only the statistical tensors of polarized intermediate ions with rank 0 and 2 contribute [24]. Therefore, due to angular momentum

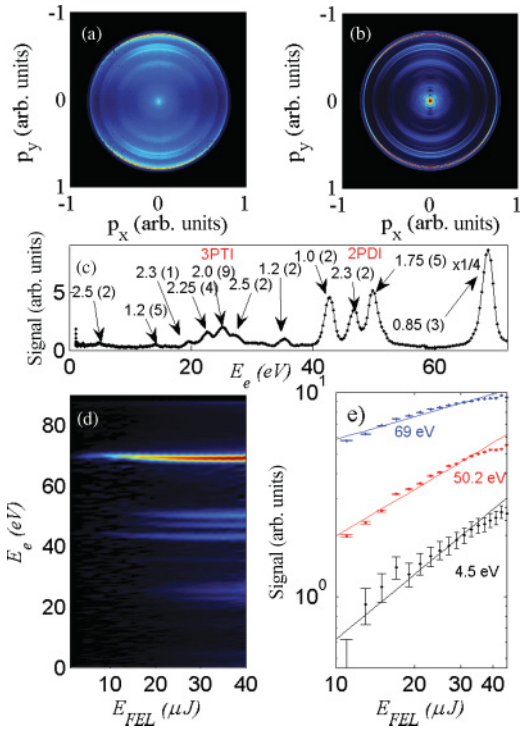

FIG. 1. (Color online) (a) Observed 2D momentum distribution and (b) 2D slice through the retrieved 3D velocity distribution. (c) Angle-integrated photoelectron spectrum obtained from panel (b). Numbers at the peaks are the exponential factors ν obtained by fits of the pulse energy dependence with the errors in the last digit shown in parentheses. (d) Evolution of the angle-integrated photoelectron spectrum with the FEL pulse energy. (e) Results of the fitting procedure for the FEL pulse energy dependence for three selected peaks in the photoelectron spectrum: 69 eV (S_1), 50.2 eV (D_2), and 4.5 eV (not labeled).

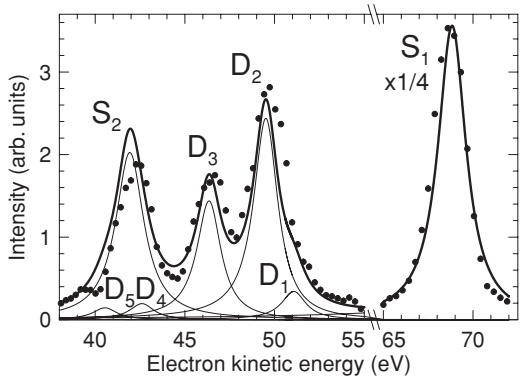

FIG. 2. Experimental (dots) and theoretical (bold line) electron spectra under the magic angle in the region above 40 eV. Thin lines indicate contributions from different processes.

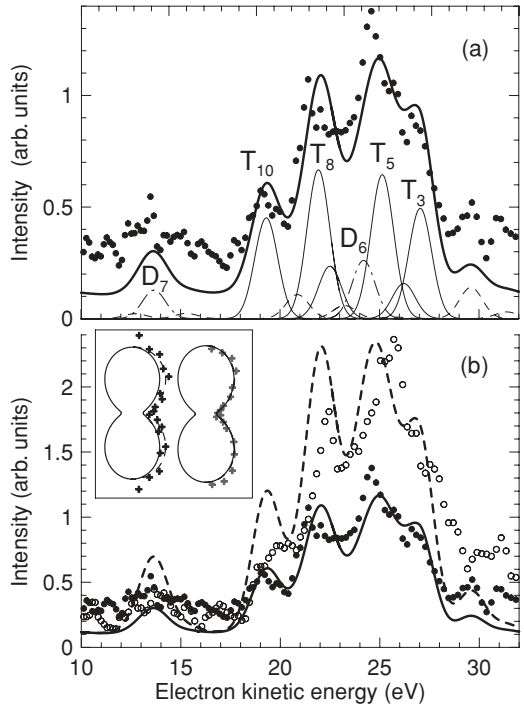

FIG. 3. Same as Fig. 2 in the region 10–32 eV. (a) Electron spectrum under the magic angle. Thin lines show the calculated contribution from the 3PTI involving only the $2p$ shell (solid), the 3PTI involving the $2s$ shell (dashed), and the 2PDI (dot-dashed). (b) Comparison of the theoretical (lines) and experimental (dots) electron spectra under zero (dashed line, open circles) and magic (solid line, black dots) angles. In the inset the polar plots show the electron angular distributions for lines T_{10} (left) and T_8 (right). Crosses: experiment, dashed line: fit, solid line: theory.

conservation, only Legendre polynomials up to fourth order enter the photoelectron angular distribution (1), i.e., $k_{\max} = 4$.

The calculated photoelectron spectrum allows one to trace a "genealogy" of the sequential photoionization: It contains "grandparent" lines (S) from single photoionization of the neutral Ne atoms, "parent" lines (D) from subsequent ionization of Ne^+ producing Ne^{2+}, and, finally, lines labeled (T) due to the production of triply charged ions Ne^{3+} from Ne^{2+}. For comparison with the experiment the theoretical single photoionization spectrum has been normalized to the intensity of the main line S_1 at 69.0 eV. The calculated spectra for the two- and three-photon processes are normalized to the intensity of the line D_3 ($Ne^+\ 2p^{5\,2}P \rightarrow Ne^{2+}\ 2p^{4\,1}D$) at 46.4 eV, and the line T_{10} ($Ne^{2+}\ 2p^{4\,3}P \rightarrow Ne^{3+}\ 2p^{3\,2}P$) at 19.4 eV, respectively. In the simulation the width of each peak was assumed to be equal to the width of the main peak S_1. The comparison of calculated and experimental spectra allowed us to identify the transitions contributing to the main spectral features shown in Figs. 2 and 3.

Consider first the high-energy part of the spectrum, displayed in Fig. 2. Apart from the strongest peak S_1, there are three other strong lines. Peak S_2 at 42.0 eV is attributed to single ionization of the $2s$ subshell, producing $Ne^+\ 2s2p^6$. The single photon character of this peak is confirmed experimentally by the slope value of 1.0(2) in the pulse energy dependence of the peak at 42.0 eV [see Fig. 1(c)]. Peaks D_2 (49.5 eV) and D_3 (46.4 eV) are the strongest contributions from sequential 2PDI and correspond to the transitions $Ne^+\ 2p^{5\,2}P \rightarrow Ne^{2+}\ 2p^{4\,3}P$ and $Ne^+\ 2p^{5\,2}P \rightarrow Ne^{2+}\ 2p^{4\,1}D$, respectively. In addition, several weaker "parent" lines originating from the "grandparents" S_1 and S_2 are observed, but their discussion is beyond the scope of this paper. The overall agreement between the calculated and experimental spectra for both the peak positions and the intensities of the peaks is good which is important since the strongest 2PDI peaks give rise to the prominent 3PTI peaks under investigation.

Figure 3(a) shows the electron spectrum at the magic angle in the low-energy region where the photoelectron lines corresponding to the sequential 3PTI should appear. The four main peaks at the energies 19.4, 22.0, 25.2, and 27.1 eV are easily attributed to the calculated 3PTI transitions T_{10} ($Ne^{2+}\ 2p^{4\,3}P \rightarrow Ne^{3+}\ 2p^{3\,2}P$), T_8 ($Ne^{2+}\ 2p^{4\,3}P \rightarrow Ne^{3+}\ 2p^{3\,2}D$), T_5 ($Ne^{2+}\ 2p^{4\,1}D \rightarrow Ne^{3+}\ 2p^{3\,2}D$), and T_3 ($Ne^{2+}\ 2p^{4\,3}P \rightarrow Ne^{3+}\ 2p^{3\,4}S$), respectively. The parent states for these lines are populated by the two strongest 2PDI processes discussed above. The relative intensity of the lines are well reproduced by the calculations. Several weaker lines, not discussed here, contribute to the complexity of the spectrum in this region.

Additional confirmation of the sequential 3PTI character of the discussed lines comes from measurements of the angular distributions. The inset in Fig. 3(b) shows a very good agreement between the experimental and calculated angular distributions for the lines T_{10} and T_8. The variation of the whole spectrum with the emission angle is demonstrated in Fig. 3(b). The agreement between theoretical and experimental spectra at two angles (0° and 54.7°) confirms our analysis. Finally, in Table I we compare the experimental and theoretical β_k parameters characterizing the angular distributions for the strongest 2PDI and 3PTI peaks. Good agreement between theory and experiment for β_2 supports our assignments. Note that β_4 is very small in both theory and experiment, and presently it can hardly be determined unambiguously.

A few other mechanisms may contribute to the photoelectron spectrum. The strongest grandparent line S_1 at 69.0 eV is accompanied by much weaker photoelectron peaks in the region of 30–40 eV due to a shake-up process producing $Ne^+\ 2p^4\,3p$. Furthermore, single-photon double ionization gives a continuous electron distribution up to 21.1, 24.8, or 28.0 eV depending on the final Ne^{2+} state, which can be $2p^{4\,1}S$, ^1D, or ^3P, respectively. Auger decay of the $Ne^+\ 2s\,2p^{\,5}nl$ states can generate electrons in the considered energy range [25] too.

TABLE I. Experimental and calculated β_2 and β_4 parameters for several strongest photoelectron lines. The estimated accuracy of the experimental values is not worse than 10%.

Line	E_e (eV)	β_2^{expt}	β_4^{expt}	β_2^{theor}	β_4^{theor}
T_{10}	19.4	0.89	−0.14	1.27	0.02
T_8	22.0	1.31	−0.04	1.33	0.03
T_5	25.2	1.29	0.05	1.33	−0.16
T_3	27.1	1.35	0.05	1.35	−0.04
D_3	46.4	1.28	0.13	1.41	0.01
D_2	49.5	1.30	0.08	1.37	−0.05

All these processes contribute to the photoelectron spectra and should be taken into account in a detailed analysis. However, our estimations show that their contribution is smaller than the dominant 2PDI and 3PTI processes.

In conclusion, sequential three-photon triple ionization of Ne atoms interacting with strong free electron laser pulses has been observed for the first time by means of angle-resolved photoelectron spectroscopy with a shot-by-shot monitoring of the FEL pulse energy. Extensive theoretical calculations of the photoelectron spectrum and the angular distributions allowed us to identify the main structures in the spectrum and to reveal the ionization mechanisms that contribute to particular photoelectron peaks. As a result of our analysis, one can attribute the sequential 3PTI as the dominant process producing triply charged ions, which can be fully understood within the conventional theory of multiphoton multiple ionization at high photon frequencies.

This work is part of the research program of the Stichting voor Fundamenteel Onderzoek der Materie (FOM), which is financially supported by the Nederlandse Organisatie voor Wetenschappelijk Onderzoek (NWO). We also acknowledge travel support from the EU under Contract RII3-CT-2004-506008 (IA-SFS) and ITN ATTOFEL. PJ acknowledges the support of the Swedish Research Council and the Swedish Foundation for Strategic Research. KU acknowledges the support from the X-ray Free Electron Laser Utilization Research Project of the Ministry of Education, Culture, Sports, Science and Technology of Japan and from the IMRAM project. EVG, ANG, and NMK acknowledge the support by the Russian Foundation for Basic Research (RFBR) under grant 09-02-00516. FB and EL acknowledge the support from the FOM Pilot project on the use of multilayer optics for FEL sources and FOM and Carl Zeiss SMT AG through the XMO IPP program. Finally, the scientific and technical team at FLASH, in particular the machine operators and run coordinators, as well as Rob Kemper, Ad de Snaijer, and Hinco Schoenmaker (AMOLF) are gratefully acknowledged for their work in preparing and installing the experimental apparatus at FLASH.

[1] H. Wabnitz, A. R. B. de Castro, P. Gürtler, T. Laarmann, W. Laasch, J. Schulz, and T. Möller, Phys. Rev. Lett. **94**, 023001 (2005).

[2] A. A. Sorokin, S. V. Bobashev, T. Feigl, K. Tiedtke, H. Wabnitz, and M. Richter, Phys. Rev. Lett. **99**, 213002 (2007).

[3] L. Young *et al.*, Nature (London) **466**, 56 (2010).

[4] M. Richter, M. Ya. Amusia, S. V. Bobashev, T. Feigl, P. N. Juranić, M. Martins, A. A. Sorokin, and K. Tiedtke, Phys. Rev. Lett. **102**, 163002 (2009).

[5] M. G. Makris, P. Lambropoulos, and A. Mihelič, Phys. Rev. Lett. **102**, 033002 (2009).

[6] A. A. Sorokin, M. Wellhöfer, S. V. Bobashev, K. Tiedtke, and M. Richter, Phys. Rev. A **75**, 051402(R) (2007).

[7] M. Braune, A. Reinköster, J. Viefhaus, B. Lohmann, and U. Becker, 2007 *International Conference on Photonic, Electronic and Atomic Collisions (ICPEAC)*, Freiburg, Germany, Book of Abstracts, Fr034.

[8] M. Kurka *et al.*, J. Phys. B **42**, 141002 (2009).

[9] R. Moshammer *et al.*, Phys. Rev. Lett. **98**, 203001 (2007).

[10] A. Rudenko *et al.*, Phys. Rev. Lett. **101**, 073003 (2008).

[11] A. Rudenko, T. Ergler, K. Zrost, B. Feuerstein, V. L. B. de Jesus, C. D. Schröter, R. Moshammer, and J. Ullrich, J. Phys. B **41**, 081006 (2008).

[12] Y. H. Jiang *et al.*, J. Phys. B **42**, 134012 (2009).

[13] A. Palasios, D. A. Horner, T. N. Rescigno, and C. W. McCurdy, J. Phys. B **43**, 194003 (2010); L. A. A. Nikolopoulos and P. Lambropoulos, *ibid.* **40**, 1347 (2007); I. A. Ivanov and A. S. Kheifets, Phys. Rev. A **75**, 033411 (2007).

[14] H. Bachau and P. Lambropoulos, Phys. Rev. A **44**, R9 (1991).

[15] P. Johnsson, W. Siu, A. Gijsbertsen, J. Verhoeven, A. S. Meijer, W. van der Zande, and M. J. J. Vrakking, J. Mod. Opt. **55**, 2693 (2008).

[16] Y. Hikosaka *et al.*, Phys. Rev. Lett. **105**, 133001 (2010).

[17] A. R. Khorsand *et al.*, Opt. Express **18**, 700 (2010).

[18] NIST Atomic Spectra Database (version 5.1.4) [http://physics.nist.gov/asd3].

[19] V. V. Balashov, A. N. Grum-Grzhimailo, and N. M. Kabachnik, *Polarization and Correlation Phenomena in Atomic Collisions. A Practical Theory Course* (Kluwer Plenum, New York, 2000).

[20] S. Fritzsche, A. N. Grum-Grzhimailo, E. V. Gryzlova, and N. M. Kabachnik, J. Phys. B **41**, 165601 (2008); **42**, 145602 (2009).

[21] E. V. Gryzlova, A. N. Grum-Grzhimailo, S. Fritzsche, and N. M. Kabachnik, J. Phys. B **43**, 225602 (2010).

[22] H. Fukuzawa *et al.*, J. Phys. B **43**, 111001 (2010).

[23] C. Froese Fischer, T. Brage, and P. Jönsson, 1997 *Computational Atomic Structure: An MCHF Approach* (IOP Publishing, Bristol, 1997).

[24] A. Verweyen, A. N. Grum-Grzhimailo, and N. M. Kabachnik, Phys. Rev. A **60**, 2076 (1999).

[25] U. Becker, O. Hemmers, B. Langer, I. Lee, A. Menzel, R. Wehlitz, and M. Ya. Amusia, Phys. Rev. A **47**, R767 (1993).